NANO LETTERS

LETTER

pubs.acs.org/NanoLett

Spin-on Spintronics: Ultrafast Electron Spin Dynamics in ZnO and $Zn_{1-x}Co_xO$ Sol−Gel Films

Kelly M. Whitaker,[†,‡,§] Maxim Raskin,[†,§] Gillian Kiliani,[†] Katja Beha,[†] Stefan T. Ochsenbein,[‡] Nils Janssen,[†,‡] Mikhail Fonin,[†] Ulrich Rüdiger,[†] Alfred Leitenstorfer,[†] Daniel R. Gamelin,[*,‡] and Rudolf Bratschitsch[*,†]

[†]Department of Physics and Center for Applied Photonics, University of Konstanz, D-78464 Konstanz, Germany

[‡]Department of Chemistry, University of Washington, Seattle, Washington 98195-1700, United States

Supporting Information

ABSTRACT: We use time-resolved Faraday rotation spectroscopy to probe the electron spin dynamics in ZnO and magnetically doped $Zn_{1-x}Co_xO$ sol−gel thin films. In undoped ZnO, we observe an anomalous temperature dependence of the ensemble spin dephasing time T_2^*, i.e., longer coherence times at higher temperatures, reaching $T_2^* \sim 1.2$ ns at room temperature. Time-resolved transmission measurements suggest that this effect arises from hole trapping at grain surfaces. Deliberate addition of Co^{2+} to ZnO increases the effective electron Landé g factor, providing the first direct determination of the mean-field electron-Co^{2+} exchange energy in $Zn_{1-x}Co_xO$ ($N_0\alpha = +0.25 \pm 0.02$ eV). In $Zn_{1-x}Co_xO$, T_2^* also increases with increasing temperature, allowing spin precession to be observed even at room temperature.

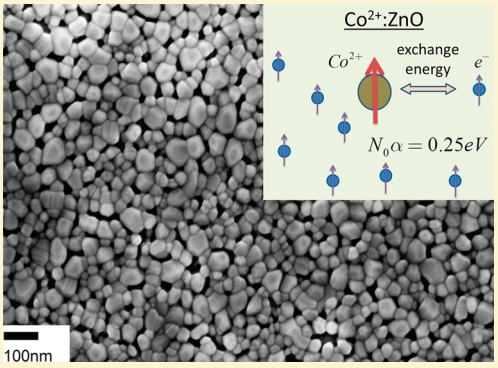

KEYWORDS: ZnCoO, sol−gel, spin dynamics, hole trapping, exchange energy, time-resolved Faraday rotation

Dopant-carrier exchange interactions in diluted magnetic semiconductors (DMSs) have been exploited to control the polarizations of carrier spins in all-semiconductor spintronics device structures such as spin light-emitting diodes and spin filters.[1] Among DMSs, n-type $Zn_{1-x}Co_xO$ has received extraordinary attention over the past decade,[2−4] ever since reports of room-temperature ferromagnetism in this material began to appear.[5] Remarkably, the magnitude of the Co^{2+}-electron exchange energy ($N_0\alpha$) has never been measured for this DMS. Magneto-optical experiments have been used to characterize the difference between Co^{2+}-electron and Co^{2+}-hole exchange energies in excitonic states, $N_0|\alpha-\beta|$, but the presence of localized midgap states complicates the analysis of magneto-optical data in this and other $Zn_{1-x}TM_xO$ DMSs substantially.[6−9] For $Zn_{1-x}Co_xO$ even the sign of $N_0(\alpha-\beta)$ remains ambiguous.[10]

Here, we describe the use of time-resolved Faraday rotation (TRFR) spectroscopy to directly probe the transient electron spin dynamics in chemically prepared ZnO and $Zn_{1-x}Co_xO$ sol−gel films. A strong dependence of the effective electron Landé g factor (g^*) on x is observed, allowing the first direct experimental measurement of both the sign and magnitude of the Co^{2+}-electron exchange energy $N_0\alpha$ in $Zn_{1-x}Co_xO$. Co^{2+} dopants greatly accelerate spin dephasing, but the sol−gel synthesis allows fine control of Co^{2+} concentrations even in the low doping regime. Coherent spin precession is observed at room temperature in all $Zn_{1-x}Co_xO$ films with doping below $x \sim 0.0025$, and the apparent spin dephasing times (T_2^*) increase with rising temperature. This anomalous temperature dependence is attributed to thermally activated hole trapping at grain surfaces, a process not seen in epitaxial thin film or bulk ZnO preparations. To our knowledge, the results presented here represent the first direct measurements of carrier spin dynamics in any member of the highly investigated $Zn_{1-x}TM_xO$ series of DMSs.

ZnO films were prepared by modification of a sol−gel synthesis method reported previously[11] (see Supporting Information for details). To fabricate $Zn_{1-x}Co_xO$ films, a fraction of the $Zn(OAc)_2$ was replaced by a stoichiometric amount of $Co(OAc)_2$. Figure 1a shows a scanning electron microscope (SEM) image of an $x = 0.0021$ $Zn_{1-x}Co_xO$ sol−gel film on sapphire with a thickness of 50 nm. It displays a columnar structure with an average grain diameter of about 50 nm. Structural investigation by X-ray diffraction demonstrates that the sol−gel films are over 98% c-plane oriented (Figure 1b). Suitability of the magnetically doped sol−gel films for optical experiments is confirmed by broadband optical transmission measurements, which show a clear onset of absorption at the fundamental bandgap (Figure 1c). Magnetization measurements at a temperature of $T = 2$ K demonstrate paramagnetic saturation behavior that was modeled using eq 1, which describes the anisotropic magnetization of Co^{2+} in the trigonal cation site of wurtzite ZnO. The first term describes the zero-field splitting, and the second models the effect of the magnetic field, oriented

Received: May 23, 2011
Revised: July 12, 2011
Published: July 12, 2011

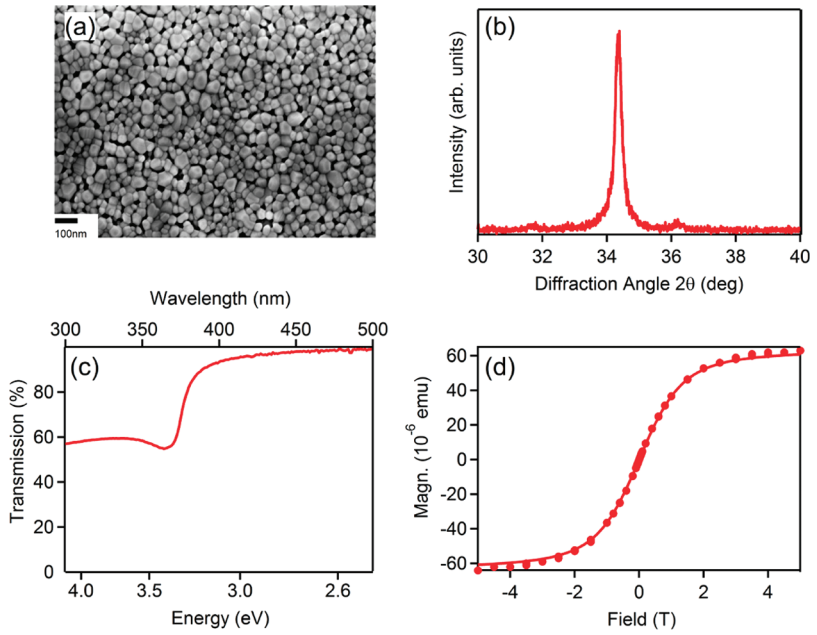

Figure 1. Structural, optical, and magnetic characterization of a $Zn_{1-x}Co_xO$ sol−gel film with a cobalt concentration of $x = 0.0021$. (a) Scanning electron microscope image, showing the granular structure of the film. (b) X-ray diffraction measurement, demonstrating over 98% *c*-plane crystal orientation. (c) Optical transmission measurement, indicating absorption at the fundamental bandgap. (d) Magnetization data recorded at $T = 2$ K using a perpendicular applied field (dots) and calculated perpendicular magnetization curve for the same conditions (line).

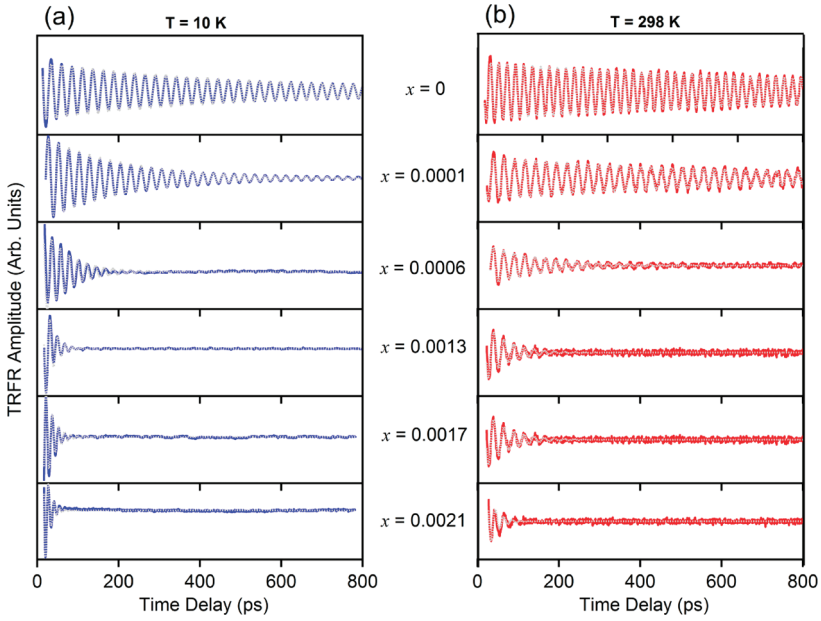

Figure 2. Time-resolved Faraday rotation traces for ZnO and $Zn_{1-x}Co_xO$ films. Time-resolved Faraday rotation data collected at (a) $T = 10$ K and (b) room temperature. The experimental data (solid lines) were recorded with a transverse magnetic field of $B_x = 1.4$ T. Laser wavelengths were $\lambda = 368$ nm at $T = 10$ K and $\lambda = 375$ nm at room temperature. Exponentially damped sinusoidal fits are displayed as gray dotted lines.

perpendicular to the *c* axis.

$$\mathscr{H} = D\left(\hat{S}_z^{\,2} - \frac{1}{3}S(S+1)\right) + g_x\mu_B B_x \hat{S}_x \qquad (1)$$

$D = 0.337$ meV is the axial zero-field splitting parameter, $\hat{S}_x$ and $\hat{S}_z$ are spin operators, $S = 3/2$ is the ground-state spin of Co^{2+}, $g_x = 2.2791$ is the in-plane *g* value of Co^{2+} in ZnO,[12] μ_B is the Bohr magneton, and B_x is the magnetic field applied perpendicular to the ZnO *c* axis. At these very low values of *x*, Co^{2+}−Co^{2+} interactions can be neglected, including potential short-range antiferromagnetic or long-range ferromagnetic coupling. The calculated magnetization curve in perpendicular orientation agrees well with the experimental data (Figure 1d).

Time-resolved Faraday rotation measurements[13−15] were performed to study the electron spin dynamics in the sol−gel

dx.doi.org/10.1021/nl201736p |*Nano Lett.* 2011, 11, 3355–3360

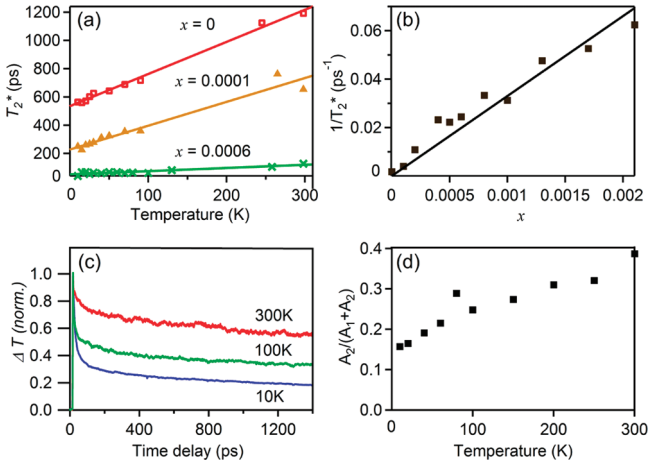

Figure 3. Dependence of electron spin dephasing times T_2^* on temperature and Co^{2+} concentration. (a) Temperature dependence of T_2^* in undoped ZnO (open red squares), $x = 0.0001$ $Zn_{1-x}Co_xO$ (filled orange triangles), and $x = 0.0006$ $Zn_{1-x}Co_xO$ (green crosses) sol−gel films. Solid lines are linear fits to the data. (b) Co^{2+} concentration dependence of $1/T_2^*$ at $T = 10$ K (filled squares), and fit to eq 5 (solid line), yielding $\tau_0 \approx 0.25$ ps. (c) Time-resolved differential transmission of the undoped ZnO film, measured at various temperatures and normalized at $t = 0$ ps time delay ($T = 10$, 100, and 300 K data shown). The curves are taken at wavelengths ranging from 375 nm ($T = 300$ K) to 368 nm ($T = 10$ K). (d) Fractional contribution of the slow carrier recombination process ($\tau_2 \sim 1700$ ps at $T = 298$ K) from panel c plotted vs temperature.

films. In this ultrafast pump−probe technique, 3 ps laser pulses in resonance with the fundamental absorption edge of the semiconductor are used to generate and probe spin-polarized excited carriers. Figure 2 shows TRFR traces of an undoped ZnO sol−gel film recorded at $T = 10$ K (Figure 2a) and room temperature (Figure 2b), along with parallel traces collected from $Zn_{1-x}Co_xO$ films at various Co^{2+} concentrations (vide infra). Exponentially damped oscillatory signals are observed that can be described using eq 2, where θ_F is the Faraday rotation angle, A is the amplitude, ω_L is the Larmor precession frequency, t is the time delay, and T_2^* is the ensemble spin dephasing time.

$$\theta_F(t) = A \exp(-t/T_2^*) \cos(\omega_L t) \quad (2)$$

From ω_L, g^* can then be determined according to eq 3.

$$g^* = \frac{\hbar\omega_L}{\mu_B B_x} \quad (3)$$

Fitting the ZnO TRFR time trace yields $g^* = 1.99$ at $T = 10$ K, which agrees well with electron g^* values for epitaxial ZnO films.[16] As reported previously,[17,18] the hole spin dephases too quickly to be observed on the picosecond time scale, so our TRFR measurements selectively probe electron spins.

Remarkably, TRFR signals in these sol−gel films persist up to room temperature and T_2^* increases with rising temperatures, in stark contrast with previous observations for epitaxial ZnO films.[16] This surprising trend is illustrated in Figure 3a, which plots T_2^* over the full temperature range between $T = 10$ and 298 K for three different sol−gel $Zn_{1-x}Co_xO$ films including $x = 0$ (undoped ZnO). In the undoped ZnO sample, T_2^* increases by over a factor of 2, from 500 ps at $T = 10$ K to more than 1 ns at room temperature. The opposite dependence of T_2^* on temperature was observed in an undoped ZnO film grown by molecular beam epitaxy (MBE) (data not shown). Sol−gel films of $Zn_{1-x}Co_xO$ show a similar temperature dependence of T_2^* as will be discussed below.

The contrast with epitaxial films suggests that the anomalous T_2^* observed in these sol−gel ZnO films arises from their granularity (Figure 1a). Hole traps at the surfaces of ZnO nanocrystals have been proposed to slow down electron−hole recombination and hence allow observation of extended electron spin coherence times.[19] We believe that this mechanism is also active in the sol−gel films studied here. To test this hypothesis, carrier recombination dynamics were probed using the same pump−probe setup by monitoring the time evolution of the transient transmission at the ZnO band-edge following photoexcitation. Figure 3c shows the differential transmission data at three different temperatures. Biphasic recombination dynamics are observed. These dynamics were fit with a biexponential function involving a short component ($\tau_1 \sim 20$ ps at $T = 10$ K, amplitude A_1), attributed to direct electron−hole recombination, and a long component ($\tau_2 \sim 700$ ps at $T = 10$ K, amplitude A_2), attributed to recombination of the conduction-band electron with a trapped hole, as discussed previously.[19] It is apparent from the transient differential transmission traces in Figure 3c that the slow component becomes more prominent as the temperature is raised. Figure 3d plots the relative amplitude of the slow component ($A_2/(A_1 + A_2)$) determined from the biexponential fitting vs temperature, which shows a steady increase with rising temperature. These data suggest that hole trapping becomes increasingly important at higher temperature, a result that implies that hole trapping is thermally activated. Although the possibility that other thermally activated processes may also contribute to this anomalous temperature dependence cannot be completely excluded, the correlation between the temperature dependence of the transient differential transmission and that of T_2^* is a strong indication that the anomalous temperature dependence of T_2^* is linked to the increasingly slow carrier recombination dynamics at elevated temperatures. The data are consistent with a picture in which electron−hole separation is thermally activated and subsequent charge recombination is slow.

Two prominent changes are observed in the TRFR signal upon precise addition of Co^{2+} to the ZnO sol−gel films (Figure 2): an increase in ω_L (i.e., an increase in g^*) and a rapid decrease in T_2^*. The inset in Figure 4a plots g^* vs x for 10 sol−gel films with different values of x, all measured at $T = 10$ K. Obviously, g^* in $Zn_{1-x}Co_xO$ can increase by a factor of almost 2 with only small changes in x. The temperature dependence of g^* was also measured (Figure 4a). In undoped ZnO, g^* remains nearly constant between $T = 10$ and 298 K ($g^* = 1.98$−2.00). In $Zn_{1-x}Co_xO$, however, g^* decreases with increasing temperature, approaching that of the undoped ZnO at high temperatures. This behavior reflects the existence of exchange coupling between the photoexcited electrons and the Co^{2+} dopants. These data therefore allow the electron−Co^{2+} exchange coupling parameter, $N_0\alpha$, for $Zn_{1-x}Co_xO$ to be determined. Because of the relationship between g^* and T_2^* found in these $Zn_{1-x}Co_xO$ films (vide infra), the data in Figure 4a were obtained by fitting just the short-time data (second oscillations) of each TRFR time trace. Within the mean-field and virtual-crystal approximations, g^* for a conduction-band electron in a DMS can be described

dx.doi.org/10.1021/nl201736p |Nano Lett. 2011, 11, 3355–3360

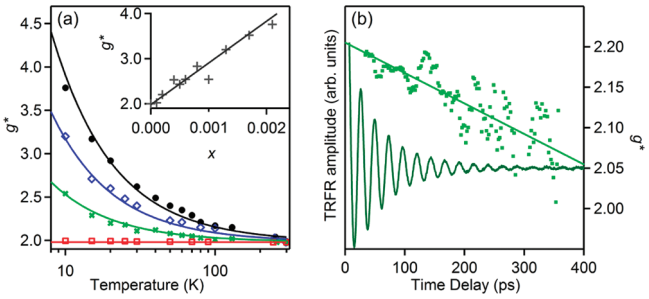

Figure 4. Temperature and time dependence of the observed effective g factor in $Zn_{1-x}Co_xO$. (a) Temperature dependence of g^* in $Zn_{1-x}Co_xO$ with x = 0.0021 (filled black circles), 0.0013 (open blue diamonds), 0.0006 (green crosses), and 0.0000 (undoped ZnO, open red squares). Inset: Dependence of g^* on Co^{2+} concentration in $Zn_{1-x}Co_xO$ sol−gel films, measured at T = 10 K. The line is calculated from eq 4 using $N_0\alpha$ = +0.25 eV. (b) Time-resolved Faraday rotation trace for the x = 0.0006 $Zn_{1-x}Co_xO$ sol−gel film, recorded at T = 25 K. The dots plot quasi-instantaneous g^* values as a function of time, and the line is a guide to the eye.

using eq 4 (ref 20).

$$g^* = g_{int} - \frac{xN_0\alpha\langle S_x\rangle}{\mu_B B_x} \tag{4}$$

The first term, g_{int}, is the intrinsic electron g value in the absence of magnetic dopants. From the undoped ZnO films, g_{int} = +1.98. The second term describes the perturbation to g^* induced by electron−Co^{2+} magnetic exchange coupling. $\langle S_x\rangle$ is the expectation value of the Co^{2+} spin perpendicular to the c axis of ZnO (i.e., along the magnetic field, B_x), and by convention is defined as a negative number. The temperature dependence of $\langle S_x\rangle$ is obtained from the numerical derivative of the eigenvalues of the axial spin Hamiltonian in eq 1 with respect to the magnetic field, weighted by the Boltzmann populations of each state.

A global fit of the data in Figure 4a yields $N_0\alpha$ = +0.25 ± 0.02 eV. The sign of $N_0\alpha$ is determined unambiguously from the observation that g^* increases rather than decreases with Co^{2+} doping (see eq 4). Curves based on this value of $N_0\alpha$ are drawn as solid lines in Figure 4a, and agree very well with the experimental data over the entire temperature and concentration ranges. The solid line in the inset of Figure 4a has a slope corresponding to $N_0\alpha$ = +0.25 eV. Hence, excellent agreement is achieved between the calculated and experimental data using $N_0\alpha$ = +0.25 eV, for all 10 samples investigated and under all experimental conditions. Note that the strong dependence of g^* on temperature makes measurements of $N_0\alpha$ by TRFR in principle susceptible to systematic error from laser heating. The measurements here were therefore all performed at the lowest possible excitation powers (55 W/cm^2 at T = 10 K) to minimize such heating effects (see Supporting Information).

To our knowledge, this is the first experimental determination of $N_0\alpha$ in $Zn_{1-x}Co_xO$. A value of $N_0|\alpha-\beta| \approx$ +0.8 eV has been reported for $Zn_{1-x}Co_xO$ MBE-grown films based on analysis of excitonic Zeeman splitting energies,[10] but the analysis is complicated by the uncertainty in the valence band ordering in ZnO[21,22] and the proximity of Co^{2+}-centered photoionization transitions[23] to the excitonic transitions. The observations of magnetoresistance and anomalous Hall effect in paramagnetic n-type $Zn_{1-x}Co_xO$ films[24] certainly indicate the existence of s−d exchange, but such data have always been analyzed[25] using $N_0\alpha$ values estimated from other Co^{2+}-based II−VI semiconductors (such as $N_0\alpha$ = +0.28 eV and +0.18 eV for $Cd_{1-x}Co_xSe$ and $Cd_{1-x}Co_xS$, respectively[26,27]). The value of $N_0\alpha$ = +0.25 ± 0.02 eV reported here is independent of the above complications and should facilitate assessment of the magneto-electronic and magneto-optical properties of this material. Recent ab initio calculations on bulk $Zn_{1-x}Co_xO$ have suggested $N_0\alpha$ = +0.34 eV (ref 6), which is in fair agreement with our experimentally determined value.

Electron spin dephasing is strongly accelerated by introduction of Co^{2+} into the sol−gel ZnO films (Figure 3b). With as little as x = 0.0001, T_2* drops from 600 to 250 ps at T = 10 K. At x = 0.0025, the TRFR signal is heavily damped with no visible oscillations remaining at T = 10 K (data not shown). Addition of Co^{2+} into the ZnO lattice clearly introduces a very effective dephasing mechanism. Nevertheless, large increases in T_2* are still visible with increasing temperatures.

The accelerated dephasing upon addition of magnetic impurities is attributed to local fluctuations of the magnetization,[28] which in turn arise from thermal fluctuations of $\langle S_x\rangle$ and from microscopically inhomogeneous spatial distributions of the dopant ions (i.e., a breakdown of the virtual crystal approximation). As in magnetic resonance spectroscopy, the efficiency of this dephasing mechanism is directly related to the strength of the exchange interaction.[29] The experimental dependence of T_2* on x shown in Figure 3b can be modeled by eq 5 (ref 28).

$$\frac{1}{T_2^*} = \frac{\gamma^2\tau_0}{N_e}\left[\langle\delta M_x^2\rangle + \langle\delta M_x^2\rangle_{cf} + \frac{(\langle\delta M_z^2\rangle + \langle\delta M_y^2\rangle)/2}{1 + (g_{int}\mu_B B_x/\hbar + \gamma\langle M_x\rangle)^2\tau_0^2}\right] \tag{5}$$

Here, $\gamma = xN_0\alpha/\hbar$ describes the interactions between the electrons and the Co^{2+} ions, τ_0 is the electron spin correlation time, $N_e = xN_0V_e$ is the average number of Co^{2+} ions within the volume of an electron (V_e), $\langle\delta M_i^2\rangle = \langle M_i^2\rangle - \langle M_i\rangle^2$ is the variance of the Co^{2+} magnetization parallel (x) and perpendicular (y, z) to the applied magnetic field due to thermal fluctuations. The average magnetization along the field also varies due to local Co^{2+} concentration fluctuations, modeled by $\langle\delta M_x^2\rangle_{cf}$. For a Poissonian distribution of dopants, $\langle\delta M_x^2\rangle_{cf}$ equals $\langle M_x\rangle$. The average magnetization $\langle M_i\rangle$ and its second moment $\langle M_i^2\rangle$ can be calculated by differentiating the eigenvalues of the axial Co^{2+} spin Hamiltonian (eq 1) with respect to the magnetic field once and twice, respectively, and weighting by the Boltzmann populations of each eigenstate. In this way, the data in Figure 3b could be fitted to eq 5 with τ_0 as the only free parameter. The solid line in Figure 3b shows the best fit, obtained using a correlation time of τ_0 = 0.25 ps. This fitted value of τ_0 is very similar to the propagation time of electrons in ZnO calculated following ref 28 ($\tau_0 \approx$ 0.1 ps), lending credence to the conclusion that the accelerated dephasing observed with increasing x is indeed caused by magnetization fluctuations.

A striking consequence of the relationship between electron−Co^{2+} coupling and electron spin dephasing is that electrons interacting with the highest number of Co^{2+} ions have the largest g^* but also dephase the quickest. Figure 4b shows a TRFR trace that illustrates this effect. Close inspection of the TRFR data for this $Zn_{1-x}Co_xO$ (x = 0.0006) sample reveals that the oscillation frequency is not constant but decreases with increasing delay times. In Figure 4b quasi-instantaneous g^* values (green dots) were extracted for single-cycle windows within this TRFR trace using an autocorrelation function. From these data, we find that

dx.doi.org/10.1021/nl201736p |Nano Lett. 2011, 11, 3355–3360

g^* decreases from 2.2 to 2.0 over the 400 ps time window of the TRFR trace. This apparent evolution of g^* reflects the fact that TRFR measures an ensemble of spins in which those with smallest g^* retain coherence longest because of the dependence of T_2^* on x described in Figure 3b.

To our knowledge, the results presented here constitute the first measurement of ultrafast carrier spin dynamics on any ZnO DMS, a class of materials that has attracted extraordinary attention in recent years for potential spintronics applications.[30−32] In both ZnO and $Zn_{1-x}Co_xO$ sol−gel films, the ensemble electron spin dephasing times T_2^* grew longer at elevated temperatures. This unprecedented behavior in ZnO-based materials is attributed to inhibition of carrier recombination via thermally activated hole trapping. Through analysis of the electron's effective g factor as a function of Co^{2+} concentration, the mean-field electron−Co^{2+} exchange coupling parameter in $Zn_{1-x}Co_xO$ has been determined for the first time ($N_0\alpha = +0.25 \pm 0.02$ eV).

A key aspect of these experiments was the ability to synthesize optical-quality $Zn_{1-x}Co_xO$ films by a rapid, inexpensive wet-chemical synthesis. This preparative approach has yielded ZnO films showing the longest room-temperature optically generated spin coherence times yet observed in any ZnO-based materials (1.2 ns). Moreover, it provided the flexibility needed to explore a broad experimental parameter space, which led to the discovery that TRFR in $Zn_{1-x}Co_xO$ could only be observed at very low values of x because of fast dephasing due to electron−Co^{2+} exchange interactions. Beyond providing fundamental new insights into the spin dynamics of ZnO DMSs, these results thus highlight the importance of exploring solution-based preparations of magnetically doped oxides for optical spin-manipulation experiments. The demonstration here that it is possible to prepare ZnO and $Zn_{1-x}Co_xO$ films suitable for optical electron spin generation and detection using rapid solution techniques, with precise control over x, marks a promising advance in the development of flexible, low-cost preparative methods for incorporation of oxide DMSs into UV optical microcavities[33] or related optoelectronic and optospintronic device structures.

■ ASSOCIATED CONTENT

Ⓢ Supporting Information. Chemical preparation of $Zn_{1-x}Co_xO$ sol−gel films, technical specifications of the setups for structural, optical, and magnetic characterization, and description of the time-resolved Faraday rotation measurement. This material is available free of charge via the Internet at http://pubs.acs.org.

■ AUTHOR INFORMATION

Corresponding Author

*E-mail: Rudolf.Bratschitsch@uni-konstanz.de; Gamelin@chem.washington.edu.

Author Contributions

§These authors contributed equally to this work.

■ ACKNOWLEDGMENT

The authors acknowledge financial support by the Deutsche Forschungsgemeinschaft (DFG) through priority program SPP 1285. Financial support from the US National Science Foundation (CHE 0628252-CRC to D.R.G.) is gratefully acknowledged. This work was supported by a grant from the Ministry of Science, Research and the Arts of Baden-Württemberg. Gillian Kiliani acknowledges the support of the Carl Zeiss Foundation.

■ REFERENCES

(1) Fiederling, R.; et al. Injection and Detection of a Spin-Polarized Current in a Light-Emitting Diode. *Nature* **1999**, *402*, 787.
(2) Kittilstved, K. R.; Liu, W. K.; Gamelin, D. R. Electronic structure origins of polarity-dependent high-T_c ferromagnetism in oxide-diluted magnetic semiconductors. *Nat. Mater.* **2006**, *5*, 291.
(3) Liu, C.; Yun, F.; Morkoç, H. Ferromagnetism of ZnO and GaN: A Review. *J. Mater. Sci: Mater. Electron.* **2005**, *16*, 555.
(4) Coey, J. M. D.; Venkatesan, M.; Fitzgerald, C. B. Donor impurity band exchange in dilute ferromagnetic oxides. *Nat. Mater.* **2005**, *4*, 173.
(5) Ueda, K.; Tabata, H.; Kawai, T. Magnetic and electric properties of transition-metal-doped ZnO films. *Appl. Phys. Lett.* **2001**, *79*, 988.
(6) Chanier, T.; Virot, F.; Hayn, R. Chemical trend of exchange coupling in diluted magnetic II-VI semiconductors: Ab initio calculations. *Phys. Rev. B* **2009**, *79*, 205204.
(7) Dietl, T. Hole states in wide band-gap diluted magnetic semiconductors and oxides. *Phys. Rev. B* **2008**, *77*, 085208.
(8) Johnson, C. A.; et al. Sub-band-gap photoconductivity in Co^{2+}-doped ZnO. *Phys. Rev. B* **2010**, *81*, 125206.
(9) Johnson, C. A.; et al. Mid-gap electronic states in $Zn_{1-x}Mn_xO$. *Phys. Rev. B* **2010**, *82*, 115202.
(10) Pacuski, W.; et al. Effect of the s,p-d exchange interaction on the excitons in $Zn_{1-x}Co_xO$ epilayers. *Phys. Rev. B* **2006**, *73*, 035214.
(11) Cao, Y.; et al. Low resistivity p-ZnO films fabricated by sol-gel spin coating. *Appl. Phys. Lett.* **2006**, *88*, 251116.
(12) Koidl, P. Optical absorption of Co^{2+} in ZnO. *Phys. Rev. B* **1977**, *15*, 2493.
(13) Awschalom, D. D.; Loss, D.; Samarth, N. *Semiconductor Spintronics and Quantum Computation*; Springer-Verlag: Heidelberg, 2002.
(14) Chen, Z.; et al. Effects of disorder on electron spin dynamics in a semiconductor quantum well. *Nat. Phys.* **2007**, *3*, 265.
(15) Chen, Z.; et al. Optical excitation and control of electron spins in semiconductor quantum wells. *Phys. E (Amsterdam, Neth.)* **2010**, *42*, 1803.
(16) Ghosh, S.; et al. Room-temperature spin coherence in ZnO. *Appl. Phys. Lett.* **2005**, *86*, 232507.
(17) Crooker, S. A.; et al. Terahertz Spin Precession and Coherent Transfer of Angular Momenta in Magnetic Quantum Wells. *Phys. Rev. Lett.* **1996**, *77*, 2814.
(18) Crooker, S. A.; et al. Optical spin resonance and transverse spin relaxation in magnetic semiconductor quantum wells. *Phys. Rev. B* **1997**, *56*, 7574.
(19) Janssen, N.; Whitaker, K. M.; Gamelin, D. R.; Bratschitsch, R. Ultrafast Spin Dynamics in Colloidal ZnO Quantum Dots. *Nano Lett.* **2008**, *8*, 1991.
(20) Furdyna, J. K. Diluted magnetic semiconductors. *J. Appl. Phys.* **1988**, *64*, R29.
(21) Reynolds, D. C.; et al. Valence-band ordering in ZnO. *Phys. Rev. B* **1999**, *60*, 2340.
(22) Lambrecht, W. R. L.; et al. Valence-band ordering and magneto-optic exciton fine structure in ZnO. *Phys. Rev. B* **2002**, *65*, 075207.
(23) Schwartz, D. A.; et al. Magnetic Quantum Dots: Synthesis, Spectroscopy, and Magnetism of Co^{2+}- and Ni^{2+}-Doped ZnO Nanocrystals. *J. Am. Chem. Soc.* **2003**, *125*, 13205.
(24) Xu, Q.; et al. Paramagnetism in Co-doped ZnO films. *J. Phys. D* **2009**, *42*, 085001.
(25) Dietl, T.; et al. Origin of ferromagnetism in $Zn_{1-x}Co_xO$ from magnetization and spin-dependent magnetoresistance measurements. *Phys. Rev. B* **2007**, *76*, 155312.
(26) Gennser, U.; et al. Exchange energies, bound magnetic polarons, and magnetization in CdSe:Co and CdS:Co. *Phys. Rev. B* **1995**, *51*, 9606.
(27) Kacman, P. Spin interactions in diluted magnetic semiconductors and magnetic semiconductor structures. *Semicond. Sci. Technol.* **2001**, *16*, R25.

(28) Rönnburg, K. E.; et al. Motional-Narrowing-Type Dephasing of Electron and Hole Spins of Itinerant Excitons in Magnetically Doped II-VI Bulk Semiconductors. *Phys. Rev. Lett.* **2006**, *96*, 117203.
(29) Slichter, C. P. *Principles of Magnetic Resonance*; Harper & Row: New York, 1963.
(30) Ohno, H.; et al. Electric-field control of ferromagnetism. *Nature* **2000**, *408*, 944.
(31) Dietl, T.; et al. Zener Model Description of Ferromagnetism in Zinc-Blende Magnetic Semiconductors. *Science* **2000**, *287*, 1019.
(32) Abolfath, R. M.; Petukhov, A. G.; Žutić, I. Piezomagnetic Quantum Dots. *Phys. Rev. Lett.* **2008**, *101*, 207202.
(33) Thomay, T.; et al. Colloidal ZnO quantum dots in ultraviolet pillar microcavities. *Opt. Express* **2008**, *16*, 9791.